Received: 27 September 2019 | Accepted: 1 November 2019

DOI: 10.1002/cta.2720

RESEARCH ARTICLE

WILEY

A buck-boost integrated high gain non-isolated half-bridge series resonant converter for solar PV/battery fed multiple load LED lighting applications

Venkata Kondala Satyakar Veeramallu | **Porpandiselvi S.** | **Narasimharaju B. L.**

Department of Electrical Engineering, National Institute of Technology, Warangal, Telangana, India

Correspondence
Venkata Kondala Satyakar Veeramallu, Department of Electrical Engineering, National Institute of Technology, Warangal 506 004, India.
Email: vvk.satyakar@student.nitw.ac.in

Summary

Solar photovoltaic (SPV) or battery fed multiple load LED lighting applications are gaining importance these days, which require independent voltage regulation and dimming control. Half-bridge resonant converters are mostly used due to their simple structure. In this paper, a buck-boost integrated high gain non-isolated symmetrical half-bridge series resonant converter is proposed for multiple load LED lighting applications. With the aid of integrated buck-boost operation, the output voltage can be regulated below and above the nominal input voltage effectively and can produce twice the gain as compared with classical half-bridge converters. Frequency modulation is implemented for output voltage regulation. Pulse width modulation (PWM) dimming has been adopted for illumination control. The proposed driver results in several advantages such as low cost, compact size, improved efficiency due to soft-switching, simple control, independent dimming, and effective operation for multiple loads. Thus, the proposed non-isolated driver configuration is well suited for SPV/battery fed multiple load LED lighting applications. The proposed configuration is tested with single LED load of 22 W and dual-LED loads of 22 W and 43 W. There is an excellent consensus between the simulation and the experimental outcomes.

KEYWORDS

buck-boost converter, LED, multiple loads, series-resonant converter, ZVS

1 | INTRODUCTION

More energy can be saved by proper utilization of electrical energy in lighting applications. Present modernization in the lighting system is replacement of traditional lighting technology with light emitting diodes (LEDs) in commercial, domestic, and industrial installations[1] due to several advantages such as long life, low maintenance, dynamic response, and high efficacy. These LED lighting systems can be fed from either DC or AC source using particular LED driver. LED driver is a converter that needs to provide desired LED voltage and ripple-free current to the LED lamp irrespective of voltage fluctuations. The performance of the LED lighting system, like overall efficiency, reliability, and lifetime, is mainly dependent on the quality of LED driver used.

Different types of converters, used as LED drivers, are available in the literature. Generally, linear regulators are used as LED drivers[2] in the earlier days. However, switched mode power converters (SMPCs) have become popular as LED drivers[3-5] as they are compact in size, low cost, and able to achieve high efficiency. But the high-frequency operation results

in increased switching losses, which demands for soft-switched LED drivers. The resonant converters are becoming more popular as they provide soft-switching, which in turn results in low EMI noise, high power density, etc. Half-bridge and full-bridge based series, parallel and series-parallel resonant converters are widely employed for LED drivers. A multi-string LED driver using full-bridge resonant converter is presented in Qu et al.[6] A novel current-controlled LED driver is proposed in Ramakrishnareddy et al[7] using full-bridge resonant converter, which demands for an additional transformer, switch, and three diodes. The input of the full-bridge series resonant converter is regulated using a buck-boost converter in Reddy et al,[8] where the power processed in buck-boost converter is low. But it requires an additional input voltage source; the buck-boost converter is hard switched and also device count is high. Several other LED driver configurations[9-14] have adopted half-bridge resonant converter due to its simple structure, easy implementation, small output filter size,[9] and high efficiency due to zero voltage switching (ZVS), etc. Further, these half-bridge resonant converters are integrated with other converters and called as a single-stage AC-DC LED drivers[15-19] that achieve multitask with reduced component count and improved efficiency.

Generally, solar photo voltaic (SPV)/battery fed LED drivers are used for low power LED lighting applications. In Alonso et al,[20] half-bridge inverter with DC blocking capacitor is used as LED driver, where inductance is varied to control the LED illumination. In Jeong et al[21] and Lin et al,[22] buck-boost integrated isolated asymmetrical half-bridge resonant converter is presented, which is suitable for wide input voltage variations. When the power processed is small and isolation is not necessary, non-isolated converters are preferred for easier implementation and less cost. In Mounika and Porpandiselvi,[12] asymmetrical duty cycle (ADC)–controlled half-bridge parallel resonant converter–based LED driver is reported. In Porpandiselvi and Mounika,[13] ADC-controlled half-bridge series resonant converter is presented for improved efficiency. In Satyakar et al,[23] buck-boost cascaded symmetrical half-bridge parallel LC resonant–based LED driver is presented for doubling the gain, but the component count is more, thus increasing overall cost and less efficient due to hard switched buck-boost converter.

LED drivers that can drive multiple loads are in need these days due to the multiusage of LED lamps in every system. Independent control of these LED lamps and independent dimming are the essential features for these drivers. Many multiple load LED drivers are available in the literature.[20,24-29] In Alonso et al,[20] the number of transformers increases as the LED loads increase. In Liu et al,[25] the number of secondary windings of transformer increases as the LED loads increase. Even though a single transformer is used in Luo et al,[26] it needs a high-frequency AC bus, along with more number of inductors and capacitors. For such lighting applications, where isolation is not significant and essential, LED drivers presented in previous works[20,25,26] may lead to increased cost. Several non-isolated LED drivers for multiple loads are reported in previous studies.[24,27-29] In Reddy and Narasimharaju,[29] the second load is driven from the leakage energy of coupled inductor used with the first load. Thus, the wattage of the second load must be less than that of the first load and hence unable to drive equal loads. In addition, the output regulation is not possible, and also, the reliability decreases for multiple loads. Further, independent dimming is not possible in Hwu and Jiang[24] and Reddy and Narasimharaju.[29] A high-efficient input-regulated multiple load LED driver is reported in Ramakrishnareddy et al[27] with reduced components. But this configuration can drive only loads with equal voltages and also independent dimming control is not possible. In Ramakrishnareddy et al,[28] the LED driver provides unequal gains for multiple loads, thus driving only loads with unequal voltages, and ZVS is achieved partially across the switching devices.

In this paper, a new buck-boost integrated high gain non-isolated symmetrical half-bridge resonant converter–based LED driver for multiple loads is proposed. As shown in Figure 1, the proposed configuration is the integration of synchronous buck-boost converter and half-bridge series LC resonant converter, which provides the same voltage gain as that of the full-bridge converter with less number of switches, effective utilization of switching devices and input voltage. The proposed configuration, when extended for multiple loads, have advantages such as ability to drive multiple loads with equal or unequal voltages/wattages, independent dimming control, etc. Thus, the proposed converter is best suitable for SPV or battery source fed multiple LED lights. The duty cycle is limited to 50% in order to achieve symmetrical operation and also to ensure ZVS operation. Due to constant LED load and small variations in the battery or SPV source, frequency modulation has been implemented to provide output voltage regulation. In addition, illumination level

FIGURE 1 Block diagram of the proposed configuration [Colour figure can be viewed at wileyonlinelibrary.com]

of LED lighting is controlled using pulse width modulation (PWM) dimming in which the average LED current is regulated without affecting the LED characteristics. This proposed converter configuration is described in detail in Section 2 . Its operating principle and analysis are explained in Section 3. The design procedure is discussed in Section 4. Simulation and practical results are discussed in Section 5. Section 6 discusses about voltage regulation and dimming techniques. In Section 7, the efficiency analysis and performance evaluation are discussed and the conclusion is presented in Section 8.

2 | PROPOSED CONVERTER

Circuit diagram of the proposed synchronous buck-boost integrated half-bridge series resonant converter–based LED driver for single load is shown in Figure 2A, where S_1 and S_2 are MOSFET switches, L_r and C_r are series resonance elements, and C_{BB} and L_{BB} are the capacitor and inductor, used under buck-boost operation, respectively. The supply voltage of the converter is V_{DC}. V_{BB} is the output voltage obtained due to buck-boost operation. i_{LBB} and i_r are the currents flowing in L_{BB} and resonant elements. v_{A1-O} and v_{A2-O} are the input and output voltages across resonant tank. The output voltage and current of LED load are represented by V_O and I_O, respectively. The proposed configuration for two loads is shown in Figure 2B, where additionally two more switches and one rectifier are added for the second load. An inherent

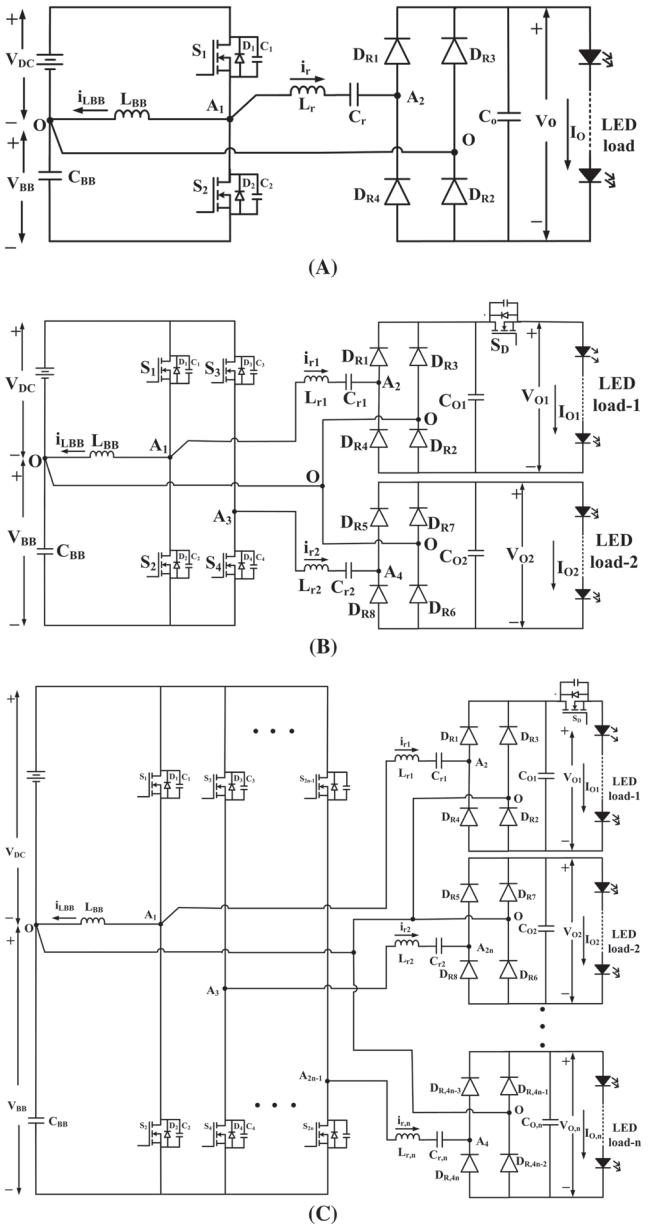

FIGURE 2 Proposed LED driver for (A) single load, (B) two loads, and (C) multiple loads

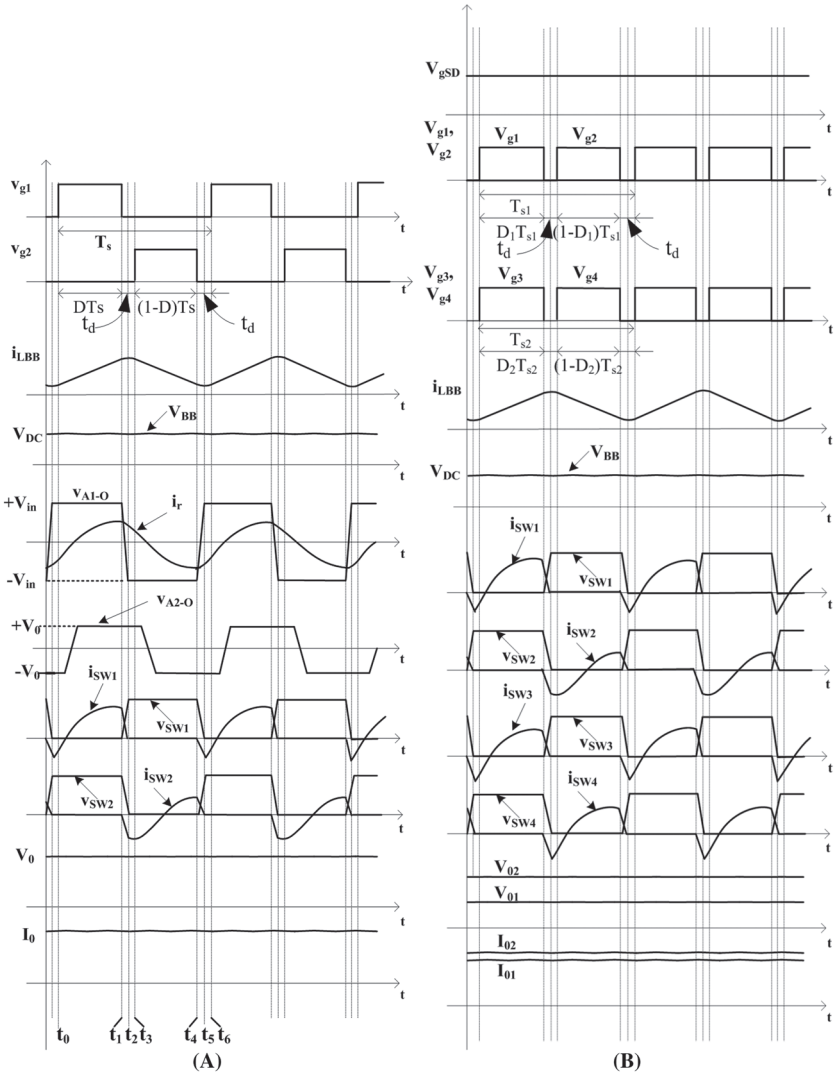

FIGURE 3 Key waveforms of proposed configuration for (A) single load and (B) two loads

dimming capability is available for load 2. But for dimming control in load 1, an external dimming switch, S_D is added in series with output as shown in Figure 2B. Thus, independent dimming control is possible with the two loads. The proposed configuration extended for multiple (n) loads is shown in Figure 2C where independent dimming and output regulation are possible. The key waveforms of proposed configuration with single load as well as two loads are shown in Figure 3A,B, respectively.

3 | OPERATING PRINCIPLE AND ANALYSIS

The principle of operation and analysis of the proposed converter with a single load and multiple loads is similar. Thus, the discussion for single load is as follows.

3.1 | Operating principle

The proposed buck-boost integrated half-bridge converter is operated with 50% duty cycle, thus providing an output voltage V_{BB} same as input voltage V_{DC}. Having two equal voltages of V_{BB} and V_{DC}, the symmetrical half-bridge resonant converter produces an output voltage (V_O) of twice than that of conventional half-bridge counterpart. Figure 3A illustrates the key waveforms of the proposed configuration, where V_{g1} and V_{g2} are the gate voltages applied to the half-bridge converter, which results in symmetrical resonance current. The fundamental component of resonant current and resonant voltages are sinusoidal in nature. The resonant current is rectified using full bridge rectifier. Finally, the rectified current, after filtering, is applied to LED load. Due to series resonance, ZVS turn OFF is achieved across the switches S_1 and S_2,

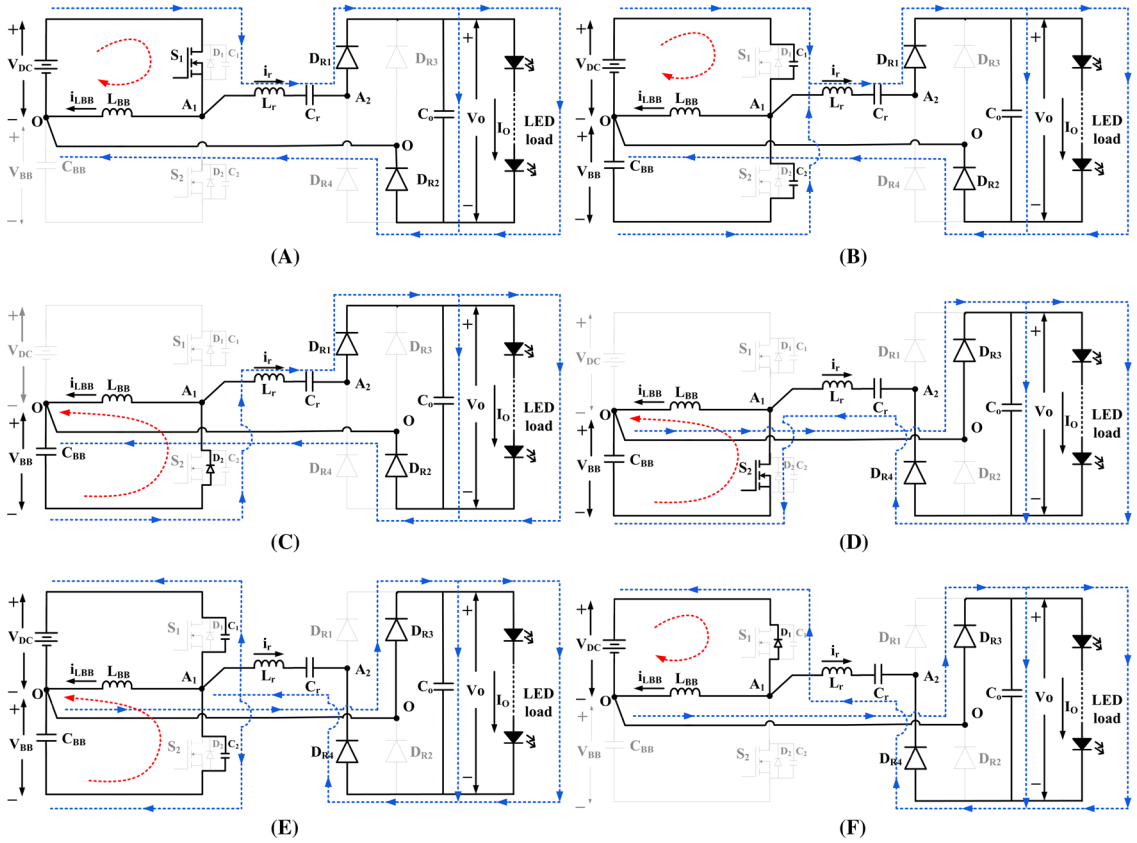

FIGURE 4 Various modes of operation of proposed converter with single load configuration: (A) mode 1, (B) mode 2, (C) mode 3, (D) mode 4, (E) mode 5, and (F) mode 6 [Colour figure can be viewed at wileyonlinelibrary.com]

thus achieving reduced switching losses and increased efficiency. With the integrated buck-boost operation, the proposed half-bridge converter is able to produce an output equal to that of full-bridge resonant converter with less switch count.

The operating modes of the proposed configuration are shown in Figure 4 and discussed as follows.

3.1.1 | Mode 1 (t_0-t_1)

Prior to this mode, D_1 is in conduction; thus, the voltage across S_1 is zero. The gate pulse is provided at t_0. As the diode current reaches zero, S_1 is turned ON with ZVS as illustrated in Figure 4A. Buck-boost inductor L_{BB} gets magnetized and current i_{LBB} raises linearly. The resonant current i_r continues to increase in positive direction. The total current flowing in the switch S_1 is given as

$$i_{S1} = i_{LBB} + i_r. \tag{1}$$

At the end of this mode, i_{LBB} reaches to its maximum value given by

$$i_{LBB\_max} = I_L + \frac{\Delta i_L}{2}, \tag{2}$$

and i_r is obtained as

$$i_r(t_1) = \left(\frac{\pi}{2}\right) I_O sin(\omega t_1 - \phi), \tag{3}$$

where

$$\phi = tan^{-1}\left(\frac{X_{Lr} - X_{Cr}}{R_{ac}}\right). \tag{4}$$

R_{ac} is the nonlinear output resistance offered by the rectifier and X_{Lr} and X_{Cr} are the reactances offered by L_r and C_r, respectively, which are expressed as

$$\left.\begin{aligned} X_{Lr} &= 2\pi f_s L_r \\ X_{Cr} &= \frac{1}{2\pi f_s C_r} \\ R_{ac} &= \frac{8}{\pi^2} R_O \end{aligned}\right\}, \tag{5}$$

where R_O is the LED output resistance.

Hence, the current i_{S1}, at the end of this mode, is given by

$$i_{S1}(t_1) = i_r(t_1) + i_{LBB\_max}. \tag{6}$$

This mode ends when switch S_1 is turned OFF.

3.1.2 | Mode 2 (t_1-t_2)

When S_1 is turned OFF at $t = t_1$, C_1 starts charging and C_2 starts discharging. Resonance occurs between these resonant capacitors and inductors L_r and L_{BB}. This duration is very short; hence, i_r is assumed to be constant and each capacitor carries half of the currents of i_r and i_{LBB} as illustrated in Figure 4B. This mode ends at $t = t_2$ when C_1 and C_2 are completely charged and discharged, respectively.

3.1.3 | Mode 3 (t_2-t_3)

At $t = t_2$, as C_2 is completely discharged to zero, D_2 becomes forward biased. The total time duration of mode 2 and mode 3 together constitute the dead time. The buck-boost inductor L_{BB} starts demagnetizing. Therefore, the current i_{LBB} decreases linearly and i_r starts decreasing. The resultant negative current due to the sum of i_{LBB} and i_r flows through D_2 as illustrated in Figure 4C. This mode ends when gate pulse is provided to S_2 at $t = t_3$.

3.1.4 | Mode 4 (t_3-t_4)

The conduction of D_2 provides ZVS turn-on of S_2. Prior to the conduction of S_2, diode D_2 current reaches to zero, and gate pulse provided at t_3; thus, S_2 is turned ON with ZVS condition. The current i_{S2} is the resultant of the two currents, i_{LBB} and i_r as illustrated in Figure 4D. At the end of this mode, the current i_r reaches to negative value given by $i_r(t_4) = -i_r(t_1)$ and i_{LBB} reaches to its minimum value given by

$$i_{LBB\_min} = I_L - \frac{\Delta i_L}{2}. \tag{7}$$

Hence, the current i_{S2}, at the end of this mode, is given by

$$i_{S2}(t_4) = -[i_r(t_4) + i_{LBB\_min}]. \tag{8}$$

This mode ends when S_2 is turned OFF at $t = t_4$.

3.1.5 | Mode 5 (t_4-t_5)

At t_4, when S_2 is turned OFF, C_1 and C_2 discharges and charges, respectively, as shown in Figure 4E. Resonance occurs due to capacitors and inductors for short duration of t_4-t_5. Hence, the resultant current is assumed constant, and each capacitor carries half of it, as illustrated in Figure 4E. This mode ends at $t = t_5$ when C_1 and C_2 are completely discharged and charged, respectively.

3.1.6 | Mode 6 (t_5-t_6)

At $t = t_5$, C_1 is completely discharged; hence, D_1 starts conducting, as shown in Figure 4F. The buck-boost inductor starts magnetizing. Therefore, i_{LBB} increases linearly, and the current i_r starts increasing from negative value. The resultant of the two currents, i_{LBB} and i_r flows through D_1 as illustrated in Figure 4F. The total duration of mode 5 and mode 6 constitutes the dead time. This mode ends when the gate pulse is provided to switch S_1 at $t = t_6$.

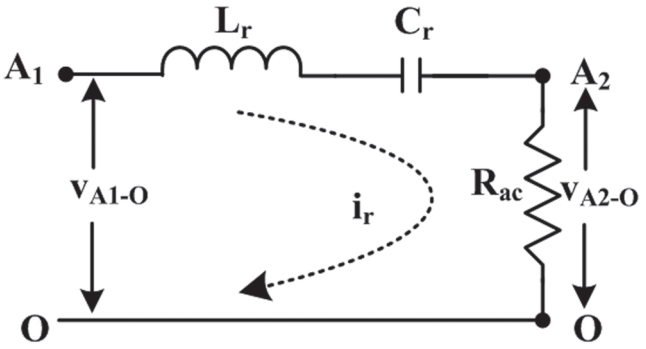

FIGURE 5 AC equivalent circuit

3.2 | Analysis of proposed converter

The assumptions considered for the analysis are as follows:

- The converter operates in steady mode.
- Power MOSFETs and diodes are ideal.
- The output voltage of the LED light is constant.

With 50% duty cycle, the integrated buck-boost operation results $V_{BB} = V_{DC}$. With two equal voltages of V_{DC} applied across half-bridge inverter, input voltage across $L_r - C_r$ network, V_{A1-O} is a square wave voltage with a peak value of V_{DC}. The static gain of the proposed resonant converter can be obtained by using conventional ac analysis in Steigerwald.[30] The AC equivalent circuit of the proposed configuration is shown in Figure 5.

From Figure 5, the static gain is expressed as

$$\frac{V_{A2-O}}{V_{A1-O}} = \frac{R_{ac}}{R_{ac} + j(X_{Lr} - X_{Cr})}, \tag{9}$$

where V_{A1-O} and V_{A2-O} are input and output voltages of the resonant network, respectively.

The static gain, in terms of converter parameters, can be expressed as

$$\frac{V_O}{V_{DC}} = \frac{1}{\left[1 + j\left(\frac{X_{Lr} - X_{Cr}}{R_{ac}}\right)\right]}. \tag{10}$$

Quality factor (Q), which measures the sharpness in the current, can be defined as

$$Q = \frac{\omega_r L_r}{R_{ac}} = \frac{1}{\omega_r C_r R_{ac}}. \tag{11}$$

The angular resonant frequency ω_r is given by

$$\omega_r = 2\pi f_r = \frac{1}{\sqrt{L_r C_r}}, \tag{12}$$

where f_r is resonant frequency in Hz. By substituting (5) and (11) into (10), the gain is obtained as

$$\frac{V_O}{V_{DC}} = \frac{1}{\left[1 + j\frac{\pi^2}{8} Q\left(\frac{f_s}{f_r} - \frac{f_r}{f_s}\right)\right]}. \tag{13}$$

The duty ratio D is expressed as

$$D = \frac{|V_{BB}|}{V_{DC} + |V_{BB}|}. \tag{14}$$

The average source current can be approximated in terms of average inductor and resonant currents as

$$I_{DC} \approx (I_{LBB} + I_r) \approx I_{LBB}. \tag{15}$$

For 100% efficiency,

$$\begin{aligned} V_{DC}I_{DC} &= V_O I_O \\ &= \frac{V_O^2}{R_O} \\ \textit{Hence}, \quad I_{DC} &= \frac{V_O^2}{V_{DC}R_O} \end{aligned} \quad . \tag{16}$$

The minimum current in L_{BB}, I_{LBBmin} can be expressed as

$$I_{LBBmin} = I_{LBB} - \frac{\Delta i_{LBB}}{2}, \tag{17}$$

where Δi_{LBB} can be expressed as

$$\Delta i_{LBB} = \frac{V_{DC}DT}{L_{BB}}. \tag{18}$$

Thus, by substituting (15), (16), and (18) in (17) and making $I_{LBBmin} = 0$, the critical inductance of buck-boost inductor, L_{BBcrit} is expressed as

$$L_{BBcrit} = \frac{V_{DC}^2 D R_O}{2V_O^2 f_s}, \tag{19}$$

where f_s is the switching frequency.

For continuous inductor current, $L_{BB} > L_{BBcrit}$.

For two loads, $D_1 = D_2 = 50\%$ and I_{DC} in (16) is modified as

$$\begin{aligned} V_{DC}I_{DC} &= V_{O1}I_{O1} + V_{O2}I_{O2} = \frac{V_{O1}^2}{R_{O1}} + \frac{V_{O2}^2}{R_{O2}} \\ \textit{Hence}, \quad I_{DC} &= \frac{V_{O1}^2 R_{O2} + V_{O2}^2 R_{O1}}{V_{DC}R_{O1}R_{O2}} \end{aligned} \quad . \tag{20}$$

Thus, L_{BBcrit} for two loads can be expressed as

$$L_{BBcrit} = \frac{V_{DC}^2 D_1 R_{O1} R_{O2}}{2(V_{O1}^2 R_{O2} + V_{O2}^2 R_{O1}) f_{s1}}. \tag{21}$$

4 | DESIGN CONSIDERATIONS

Figure 6 shows the symbol and equivalent circuit of LED, which comprises LED cut-in or threshold voltage V_{th} in series with its dynamic resistance r_d and an ideal diode. TMX HP3W white LEDs are used in the experimental prototype. The threshold voltage of each LED is 2.321 V. In order to realize the LED lamp of 22.77 W and 22.505 V with a current of 1.012 A and having a threshold voltage of 16.247 V, the operating point of LED is selected as 3.215 V and 506 mA. Thus, the total LED load comprises two LED strings in parallel where each string contains seven LEDs in series.

4.1 | Selection of input dc voltage, V_{DC}

To achieve the output voltage V_O of 22.5 V, the input voltage V_{DC} is computed as 48 V from (13) with the chosen Q-factor and frequency ratio $\left(\frac{f_s}{f_r}\right)$ values of 4.14 and 1.2, respectively.

4.2 | Calculation of L_{BB}

By using (14) and (19), the inductance L_{BBcrit} is calculated, and to maintain the continuous conduction and reduced peak current in switches, inductance L_{BB} is chosen higher than L_{BBcrit} as 120μH.

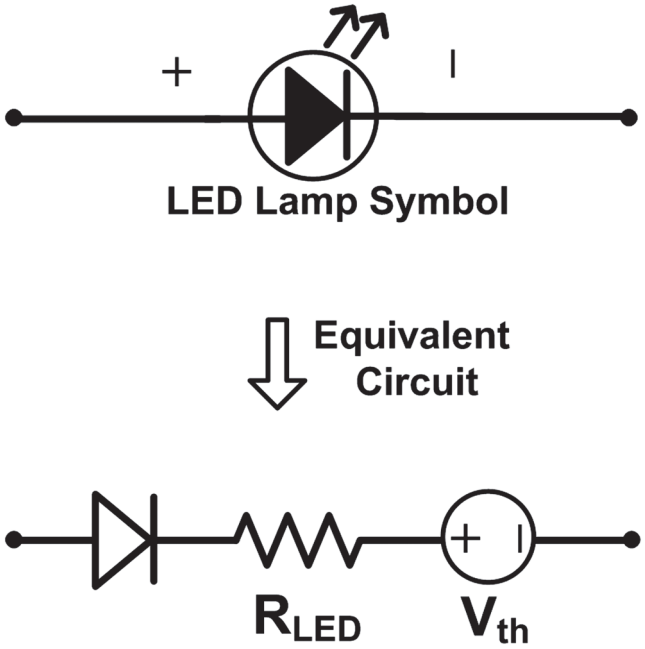

FIGURE 6 LED symbol and its equivalent circuit

4.3 | Calculation of resonant elements

The product of L_r and C_r is obtained from (12), and it is expressed as

$$L_r C_r = \left[\frac{1}{2\pi f_r}\right]^2. \tag{22}$$

With f_s of 200 kHz and the ratio f_s/f_r as 1.2, (22) can be expressed as

$$L_r C_r = 0.91344 \times 10^{-12}. \tag{23}$$

From (23), the elements L_r and C_r are selected as 88μH and 10.31 nF, respectively.

Further, the proposed configuration is also extended and tested for two different LED loads with load 1 of 22.5 W and load 2 of 43 W. The schematic of extended two load configuration is illustrated in Figure 2B, and its design is similar to the single load configuration. The first load considered is the same load that is used in the single load configuration. In order to design the second LED load for 43.41 W and 39.612 V with a current of 1.096 A and threshold voltage of 27.852 V, the operating point of LED is selected as 3.301 V and 548 mA. Thus, the total LED load 2 comprises two LED strings in parallel where each string contains 12 LEDs in series. After computing L_{BBcrit} with two loads from (21), the value of inductor L_{BB} is chosen little higher than L_{BBcrit} as 50μH.

5 | SIMULATION AND EXPERIMENTAL RESULTS

To confirm the feasibility of the proposed configuration, a prototype has been built and tested with a single load of 22.5 W and with two loads of 22.5 and 43 W. Table 1 shows the parameters of the proposed LED driver for single load as well as two loads. The experimental results are validated with OrCAD PSpice simulation counterparts. Figure 7A shows the experimental setup of the proposed LED driver. The control logic is implemented using PWM ICs as shown in Figure 7B.

The simulation and experimental results of the proposed configuration with single load for 100% dimming are shown in Figures 8 to 10. Figure 8A,C depicts the simulation and experimental waveforms of i_{LBB} and V_{BB}, which is evident that $V_{BB} \approx V_{DC}$ with 50% duty cycle. Figure 8B,D shows the simulation and experimental waveforms of i_r and v_{A1-O}. Figure 9 shows the simulation and experimental waveforms of switch voltages and currents, which evidences the ZVS turn-off of all switches. It can also be noticed from Figure 9 that peak currents in both switches are not similar, as these switches carry the resultant current due to i_{LBB} and i_r. Figure 10A,B shows the simulation and experimental waveforms of V_O and I_O at full illumination level.

TABLE 1 Design parameters

	Parameters	Values for Single Load	Values for Two loads
Input	DC input voltage	$V_{DC} = 48$ V	$V_{DC} = 48$ V
Common	Buck-boost inductor	$L_{BB} = 120$ µH	$L_{BB} = 50$ µH
	Buck-boost capacitor	$C_{BB} = 10$ µF	$C_{BB} = 10$ µF
Devices used	Switching devices	IRF 540N	IRF 540N
	Power diodes	MBR20200CT	MBR20200CT
Load 1	Switching frequency	$f_s = 200$ kHz	$f_{s1} = 200$ kHz
	Output voltage	$V_O = 22.5$ V	$V_{O1} = 22.5$ V
	Output current	$I_O = 1.012$ A	$I_{O1} = 1.012$ A
	Output power	$P_O = 22.77$ W	$P_{O1} = 22.77$ W
	Resonant frequency	$f_r = 166.53$ kHz	$f_{r1} = 166.53$ kHz
	Resonant inductor	$L_r = 88$ µH	$L_{r1} = 88$ µH
	Resonant capacitor	$C_r = 10$ nF	$C_{r1} = 10$ nF
	Output capacitor	$C_O = 4$ µF	$C_{O1} = 4$ µF
	Dimming frequency	$f_{Dim} = 200$ Hz	f_{Dim1} 200 Hz
Load 2	Switching frequency	NA	f_{s2} 200 kHz
	Output voltage		$V_{O2} = 39.6$ V
	Output current		$I_{O2} = 1.096$ A
	Output power		$P_{O2} = 43.41$ W
	Resonant frequency		$f_{r2} = 178.63$ kHz
	Resonant inductor		$L_{r2} = 77$ µH
	Resonant capacitor		$C_{r2} = 10$ nF
	Output capacitor		$C_{O2} = 4$ µF
	Dimming frequency		$f_{Dim2} = 200$ Hz

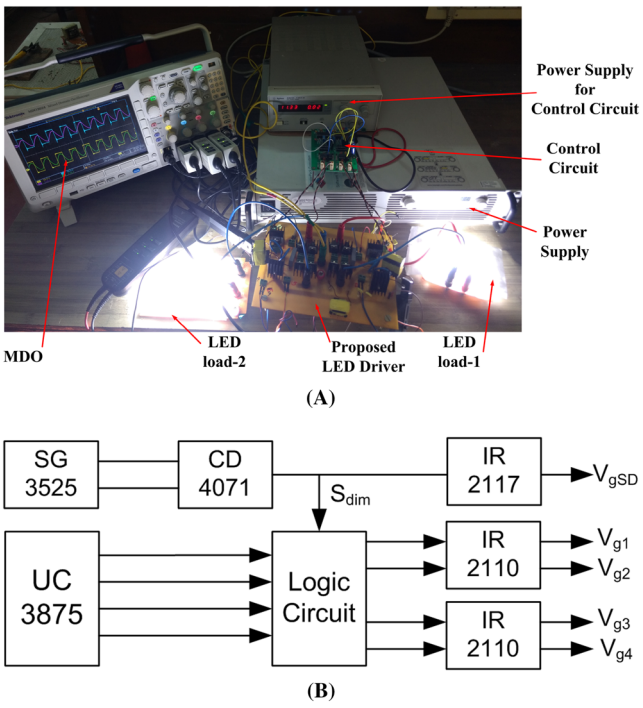

FIGURE 7 (A) Experimental setup of proposed configuration. (B) Schematic of the control circuit [Colour figure can be viewed at wileyonlinelibrary.com]

For two load configurations, shown in Figure 2B, in order to operate for full illumination level, the dimming switch S_D must be always ON as shown in Figure 3B. The simulation and experimental results of the proposed configuration for two loads with 100% dimming are shown in Figures 11 to 15. Figure 11 shows the simulation and experimental waveforms of V_{BB} and i_{LBB}. Figure 12A,B shows the simulation and experimental waveforms of the resonant currents and voltages of the two loads. Figure 13A shows the simulation waveforms of S_1 and S_2 voltages and currents. The corresponding experimental waveforms are shown in Figure 13B. ZVS turn-off across both the switches can be observed. Figure 14A shows simulation waveforms of S_3 and S_4 voltages and currents, and the experimental waveforms are shown in Figure 14B.

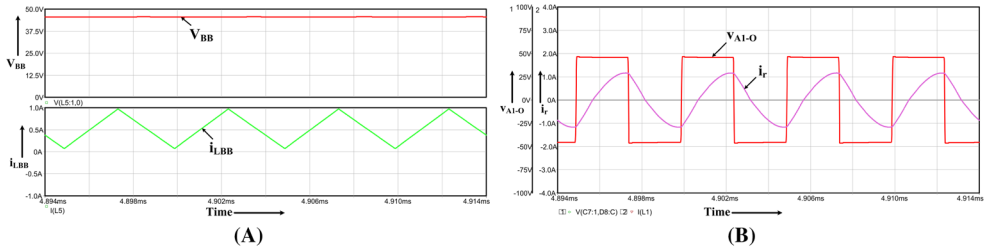

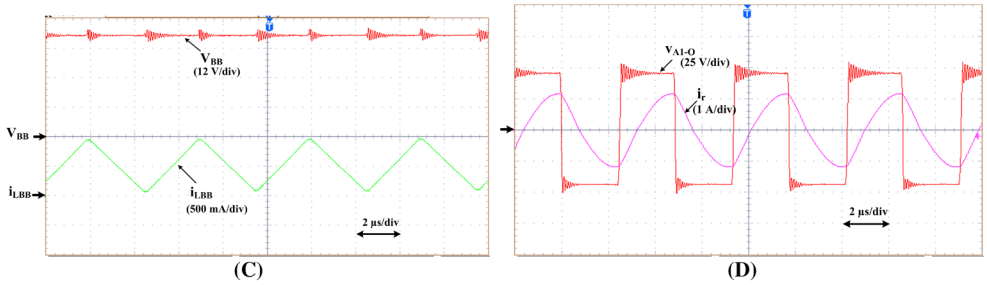

FIGURE 8 Waveforms with single load configuration: (A) simulation waveforms of V_{BB} and i_{LBB}, (B) simulation waveforms of V_{A1-O} and i_r, (C) experimental waveforms of V_{BB} and i_{LBB}, (D) experimental waveforms of V_{A1-O} and i_r [Colour figure can be viewed at wileyonlinelibrary.com]

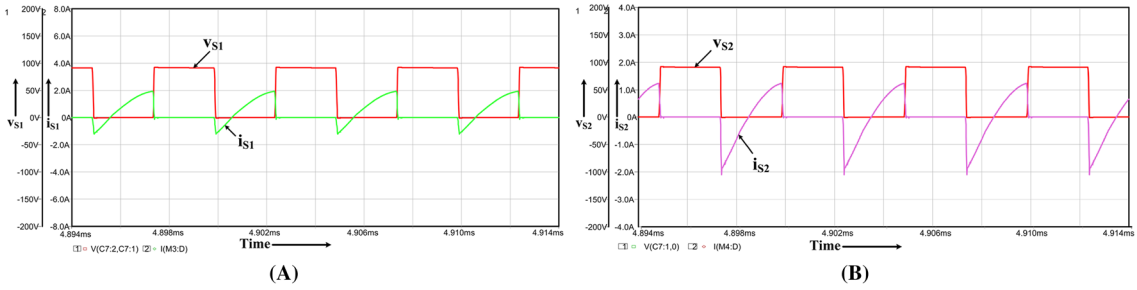

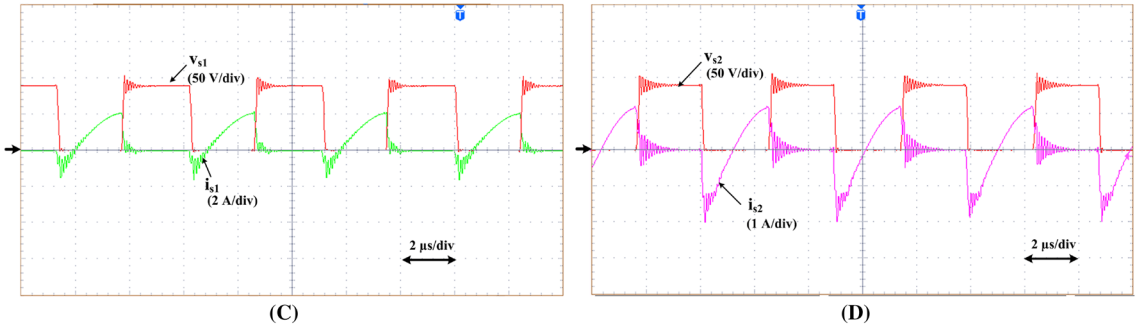

FIGURE 9 Waveforms of switch current and voltages with single load: (A) simulation waveforms of switch S_1, (B) simulation waveforms of switch S_2, (C) experimental waveforms of switch S_1, (D) experimental waveforms of switch S_2 [Colour figure can be viewed at wileyonlinelibrary.com]

ZVS turn-off across both the switches can be observed. The peak values of currents in S_1 and S_2 are not similar, as they carry both i_{LBB} and i_{r1}. But S_3 and S_4 carry only i_{r2} and no effect of buck-boost inductor current i_{LBB}, thus resulting in equal peak currents. Figure 15A,B shows the simulation and experimental waveforms of output voltage and currents of load 1 and load 2 at full illumination level.

6 | REGULATION OF ILLUMINATION AND LED VOLTAGE

In the proposed configurations, inverter switches are operated with 50% duty cycle. The output LED load voltage is regulated using frequency control against input voltage variations. The proposed converter is tested for input voltage variations from 44 to 52 V. Table 2 shows the corresponding frequency control with a single load and two loads. With two loads, independent control of voltage regulation is possible by controlling the switching frequency of switching devices of the corresponding inverter leg. For example, as shown in Table 2, when $V_{DC} = 44V$, f_{S1} of 196 kHz and f_{S2} of 194 kHz are

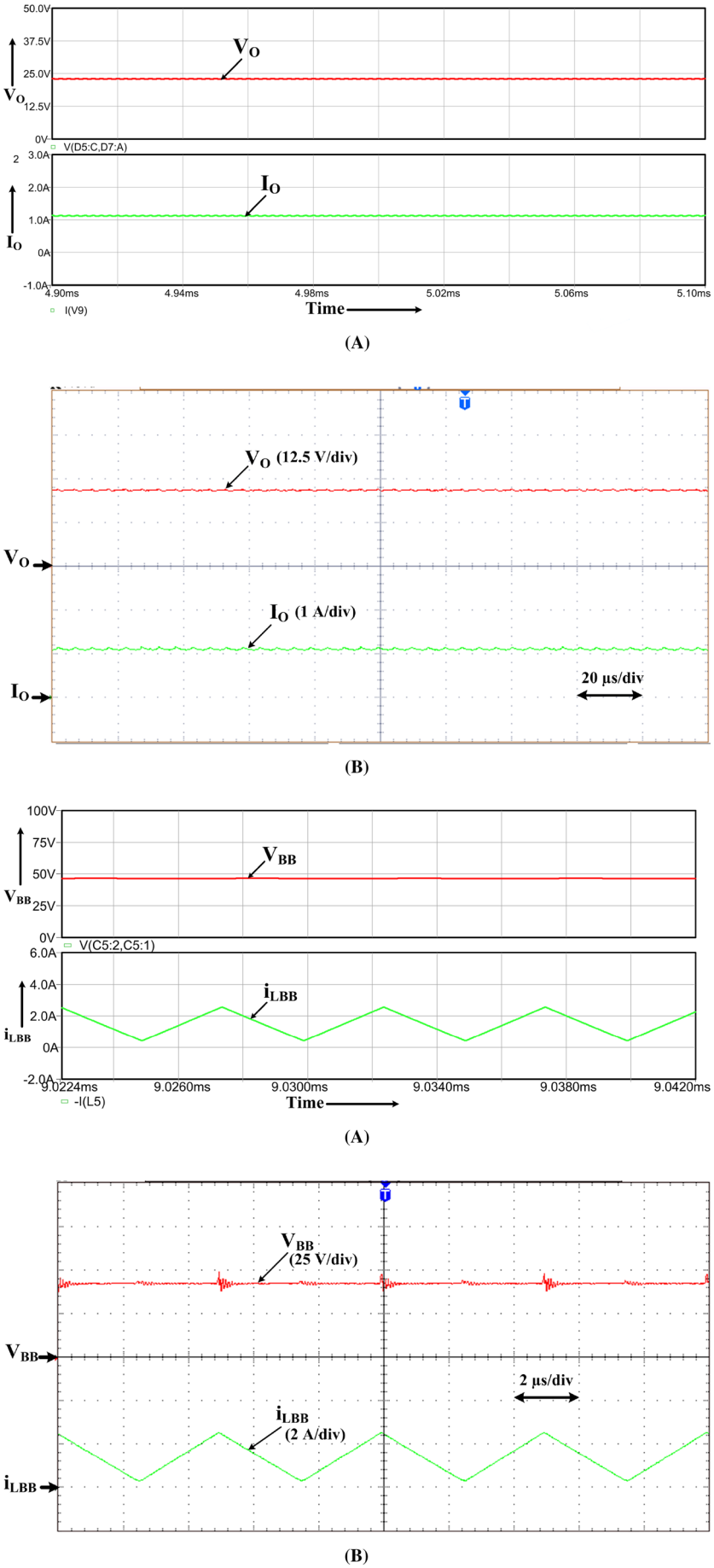

FIGURE 10 Waveforms of LED output voltage and current with single load: (A) [Colour figure can be viewed at wileyonlinelibrary.com]

FIGURE 11 Waveforms of V_{BB} and i_{LBB} for two load configuration: (A) simulation, (B) experimental [Colour figure can be viewed at wileyonlinelibrary.com]

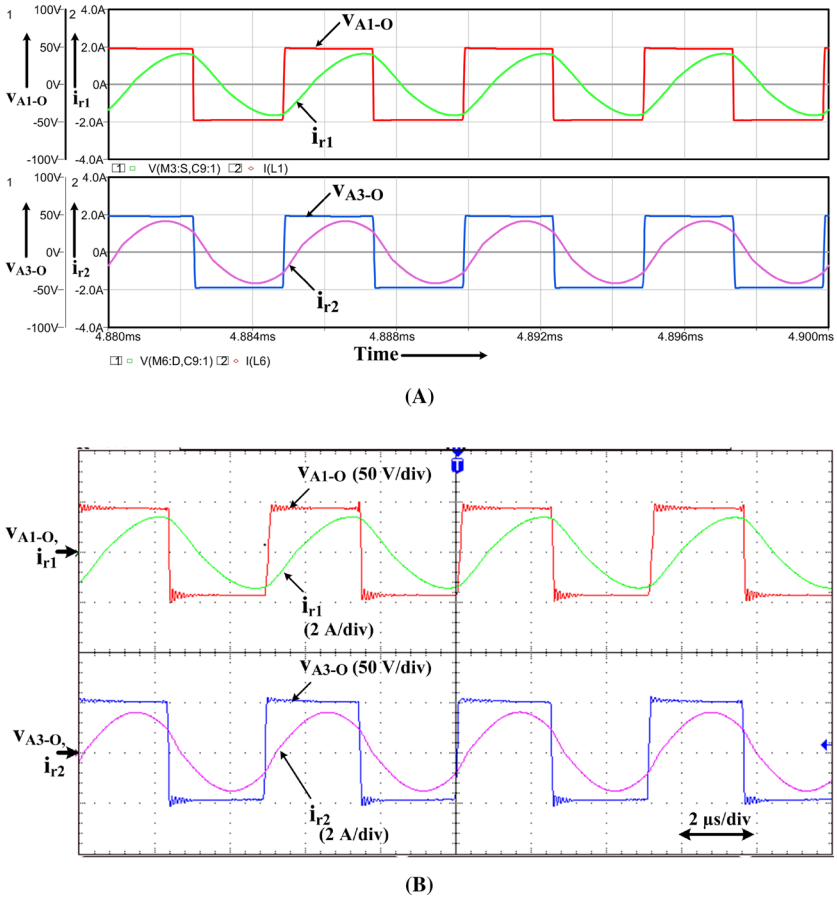

FIGURE 12 Waveforms of resonant current and voltages of load 1 and load 2: (A) simulation, (B) experimental [Colour figure can be viewed at wileyonlinelibrary.com]

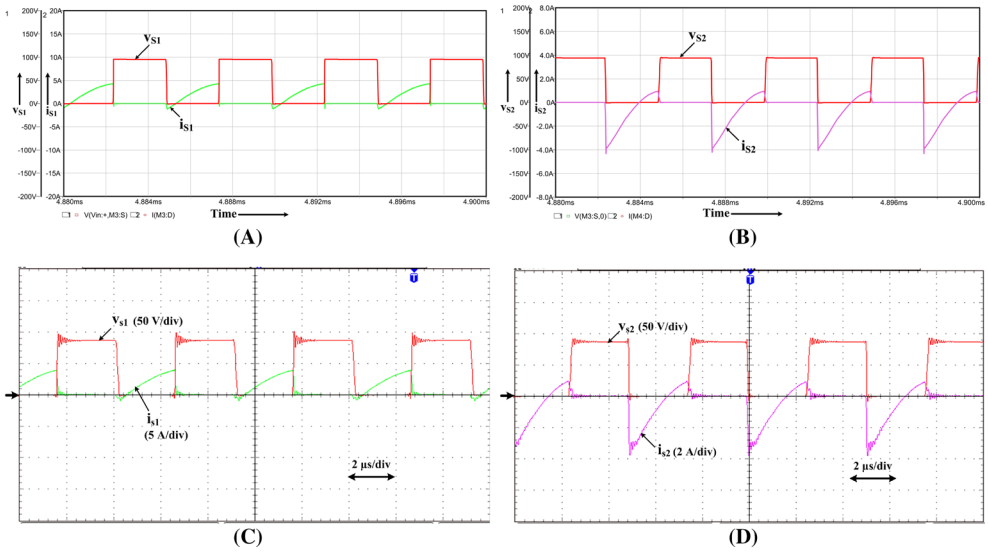

FIGURE 13 Waveforms of inverter switch current and voltages of load 1: (A) simulation waveforms of switch S_1, (B) simulation waveforms of switch S_2, (C) experimental waveforms of switch S_1, (D) experimental waveforms of switch S_2 [Colour figure can be viewed at wileyonlinelibrary.com]

required to maintain constant voltages in load 1 and load 2, respectively. Thus, independent output voltage regulation is possible with the proposed configuration.

Further, a low frequency (200 Hz) PWM dimming is implemented for illumination control, as illustrated in Figure 16, where δ_d and T_d are duty cycle and time period of dimming signal, respectively. Thus, controlling the δ_d from 20% to 100%, the average current in the LED lamp is regulated without affecting the operating point of LED lamp. Figure 16 depicts the schematic waveforms under dimming for single load. From Figure 16, it can be observed that V_O reduces below threshold voltage when input voltage for resonant tank V_{A1-O} is zero and thereby I_O reduces to zero. Figures 17 and 18

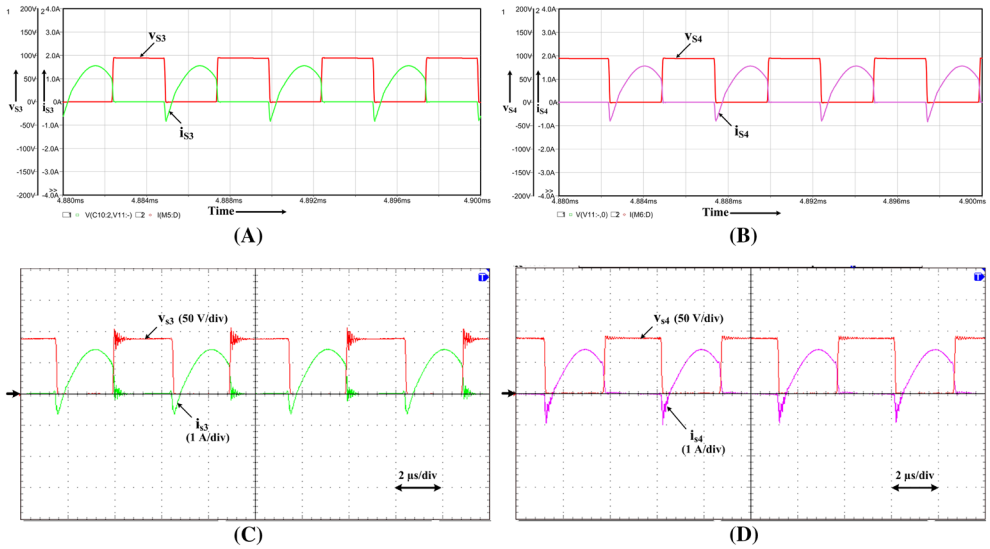

FIGURE 14 Waveforms of inverter switch current and voltages of load 2: (A) simulation waveforms of switch S_3, (B) simulation waveforms of switch S_4, (C) experimental waveforms of switch S_3, (D) experimental waveforms of switch S_4 [Colour figure can be viewed at wileyonlinelibrary.com]

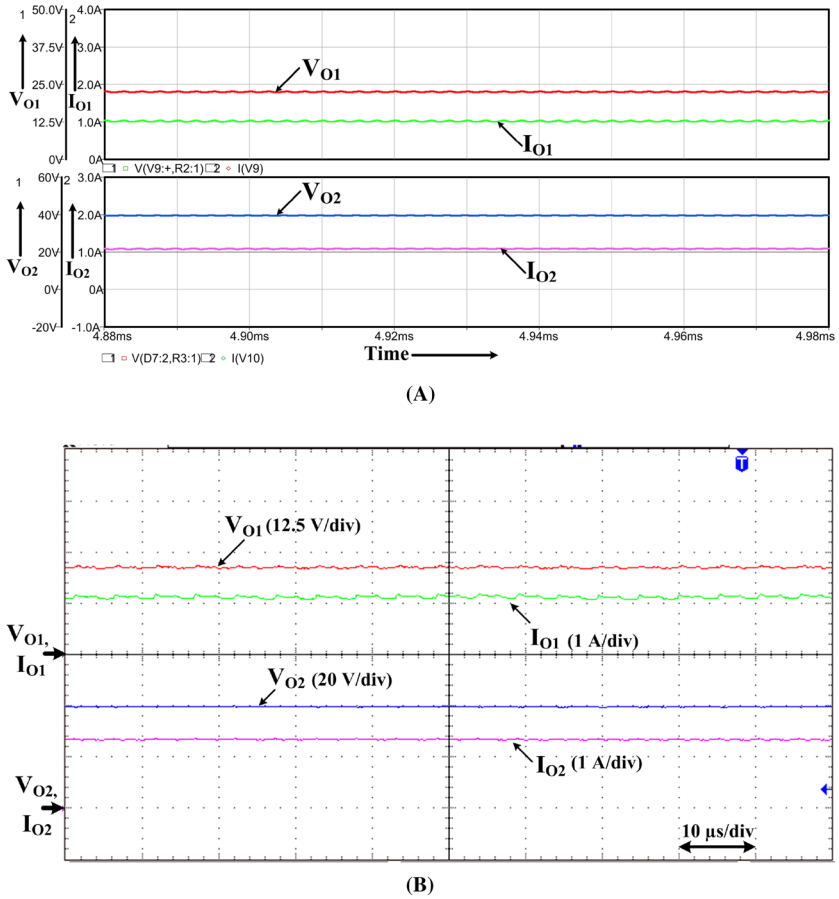

FIGURE 15 Waveforms of LED output voltage and current of both loads: (A) simulation, (B) experimental [Colour figure can be viewed at wileyonlinelibrary.com]

show the simulation and experimental waveforms of i_{LBB}, V_{BB}, V_O, and I_O at 40% and 80% dimming levels dimmed with a low dimming frequency of 200 Hz.

Schematic waveforms of dimming signals for two loads is shown in Figure 19. When the dimming level of load 1 is equal to or greater than the dimming level of load 2, the inverter leg of a particular load is turned ON-OFF based on required dimming levels. The input voltages for load 2 are V_{DC} and V_{BB}; buck-boost operation is always essential for the operation of load 2. Hence, for effective operation of load 2, the switches (S_1 and S_2) integrated with buck-boost operation should be always ON. Thus, to control the dimming operation of load 1 for lower dimming level than load 2 counterpart, the switch S_D is turned ON-OFF with low dimming frequency as shown in Figure 19B. Thereby, independent dimming

is possible with both loads. Figures 20 and 21 show the simulation and experimental waveforms of LED output voltage and currents of two loads with equal and unequal dimming levels, respectively. Figure 20 shows dimming waveforms with equal dimming levels. Figure 20A,C shows the simulation and experimental dimming waveforms with 40% dimming. Figure 20B,D shows the simulation and experimental dimming waveforms with 70% dimming. Figure 21 shows the dimming waveforms with independent dimming levels. Figure 21A,C shows the simulation and experimental dimming waveforms when load 1 operated with 70% dimming and load 2 operated with 40% dimming. Figure 21B,D shows the simulation and experimental dimming waveforms when load 1 operated with 40% and load 2 operated with 70% dimming, respectively. Thereby, independent dimming is also achieved across the two loads using the proposed configuration.

7 | EFFICIENCY AND COMPARISON

In order to maintain constant output voltage against input voltage variations, frequency control is employed in the proposed configuration. Figure 22A shows the efficiency curve with frequency control for a single load. Efficiency is above 91% for the entire frequency range, and maximum efficiency is 93.23%. Figure 22B shows the efficiency curve for different dimming levels, where the proposed converter maintains high efficiency of 93% to 94% at all dimming levels. The two load configuration also provides an overall high efficiency of 92.3%.

When compared with conventional half-bridge converter, the proposed configuration doubles its gain with an extra inductor for single load. However, only one additional dimming switch is required to achieve independent dimming control of multiple loads. When compared with conventional full-bridge converter, the proposed configuration reduces the switch count by $(2n-1)$ where n is number of loads. In Satyakar et al,[23] non-isolated LED driver is proposed with high

TABLE 2 Regulation of output current with the variation of switching frequency for input voltage variations

Variation of V_{DC}, V	Single Load	Two Loads	
	f_s, kHz	f_{s1}, kHz	f_{s2}, kHz
52	204	204	206
50	202	202	203
48	200	200	200
46	198	198	197
44	196	196	194

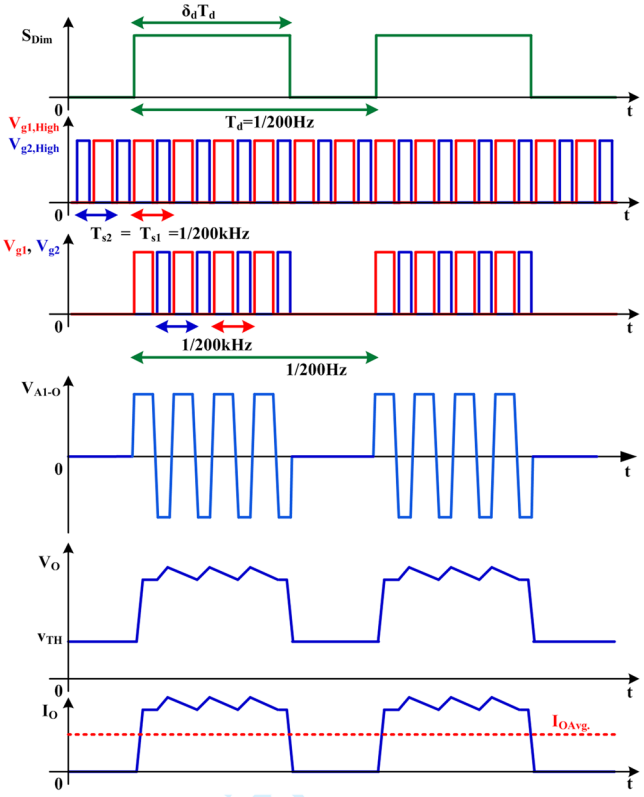

FIGURE 16 Dimming control of the proposed converter for a single load [Colour figure can be viewed at wileyonlinelibrary.com]

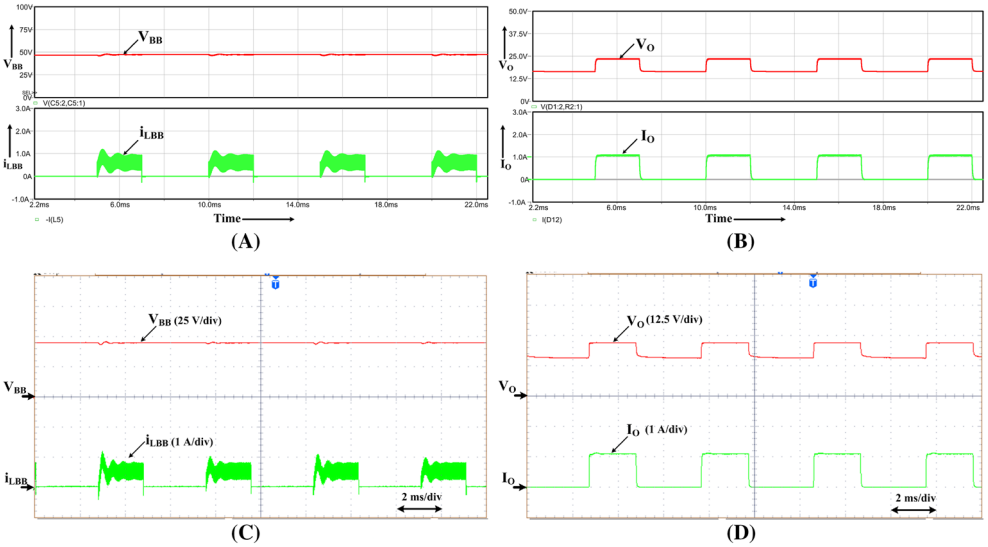

FIGURE 17 Dimming waveforms at 40% dimming with single load configuration: (A) simulation waveforms of V_{BB} and i_{LBB}, (B) simulation waveforms of V_O and I_O, (C) experimental waveforms of V_{BB} and i_{LBB}, (D) experimental waveforms of V_O and I_O [Colour figure can be viewed at wileyonlinelibrary.com]

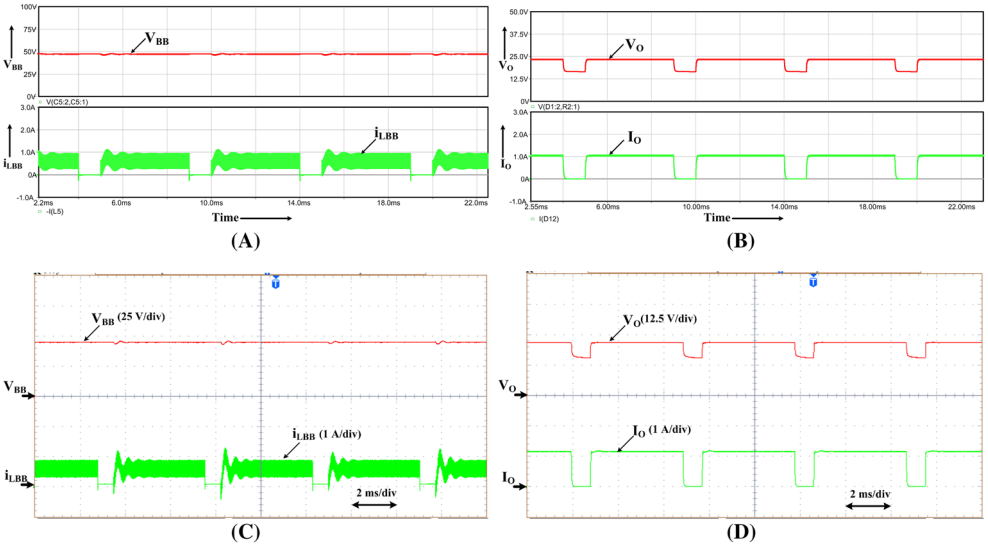

FIGURE 18 Dimming waveforms at 80% dimming with single load configuration: (A) simulation waveforms of V_{BB} and i_{LBB}, (B) simulation waveforms of V_O and I_O, (C) experimental waveforms of V_{BB} and i_{LBB}, (D) experimental waveforms of V_O and I_O [Colour figure can be viewed at wileyonlinelibrary.com]

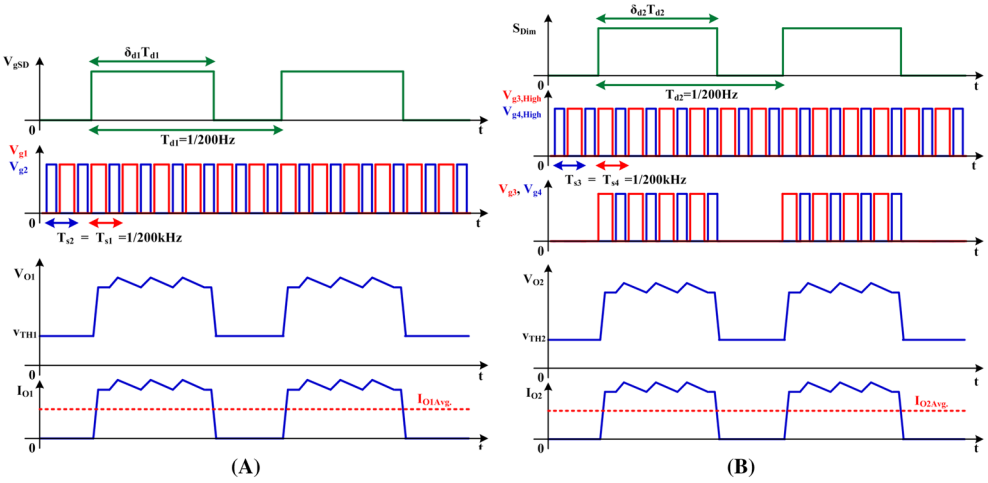

FIGURE 19 Dimming control of the proposed converter for two loads: (A) for load 1, (B) for load 2 [Colour figure can be viewed at wileyonlinelibrary.com]

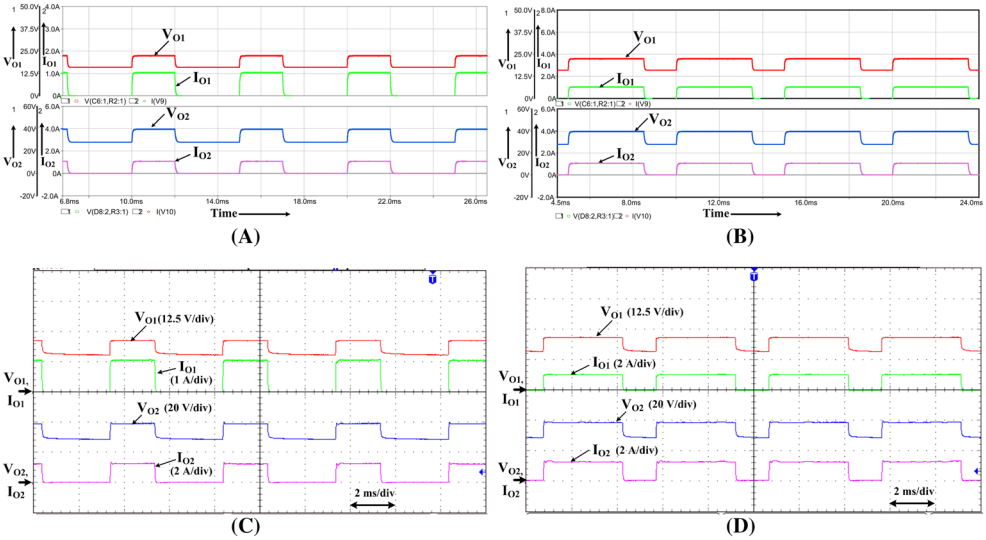

FIGURE 20 Dimming waveforms of V_{O1}, I_{O1}, V_{O2} and I_{O2} for two load configuration with equal dimming levels: A, Simulation waveforms at 40% dimming B Simulation waveforms at 70% dimming C, Experimental waveforms at 40% dimming D, Experimental waveforms at 70% dimming [Colour figure can be viewed at wileyonlinelibrary.com]

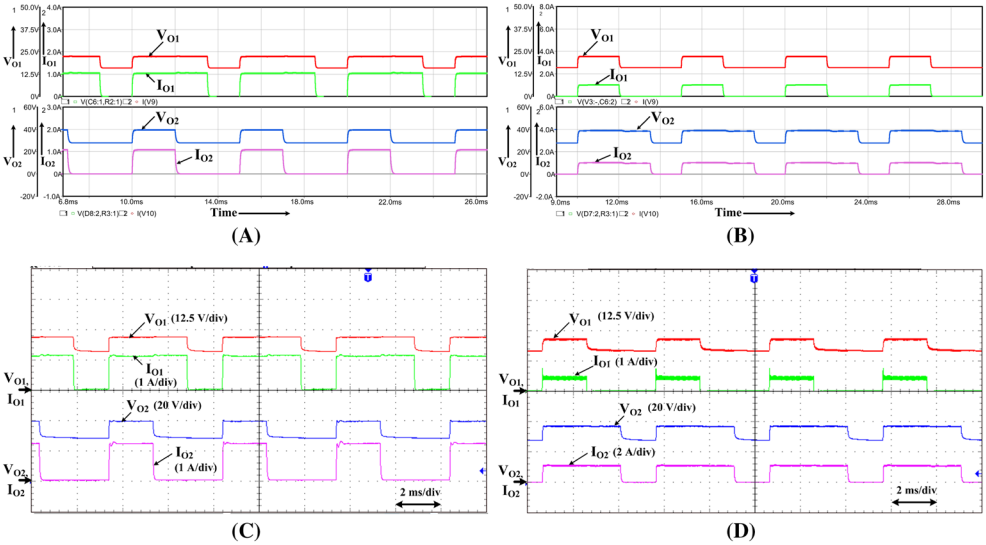

FIGURE 21 Dimming waveforms of V_{O1}, I_{O1}, V_{O2} and $_2$ for two load configuration with unequal dimming levels: A, Simulation waveforms with load-1 70% and load-2 40% dimming B, Simulation waveforms with load-1 40% and load-2 70% dimming C, Experimental waveforms with load-1 70% and load-2 40% dimming D, Experimental waveforms with load-1 40% and load-2 70% dimming [Colour figure can be viewed at wileyonlinelibrary.com]

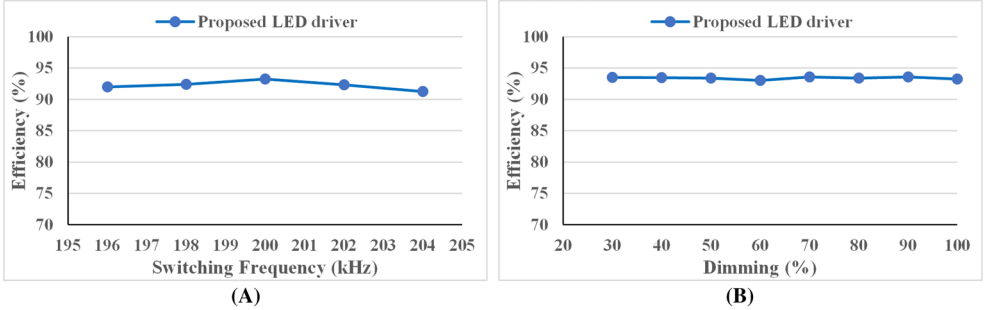

FIGURE 22 Efficiency curves: A, Efficiency vs switching frequency B, Efficiency vs dimming level [Colour figure can be viewed at wileyonlinelibrary.com]

TABLE 3 Comparison of proposed configuration with existing similar multiple load LED drivers

Features	Liu et al[25]	Reddy and Narasimharaju[29]	Alonso et al[20]	Hwu and Jiang[24]	Ramakrishnareddy et al[27]	Luo et al[26]	Ramakrishnareddy et al[28]	Proposed
ZVS	Yes	Yes	Yes	No	Yes	Yes	Yes	Yes
Input voltage, V	48	150	380	12	66	400	48	48
Total output power, W	20	30	50	24	145	200	126	65
Peak efficiency, %	93.4	95.5	90.5	91.7	94.96	92.8	92.45	92.3
No. of switches (multiple loads, n)	$2+n$	n	2	2	$2+n$	4	2+2n	1+2n
No. of diodes (multiple loads, n)	$4n$	n	$2n$	$2n$	1	4n	4n	4n
No. of inductors (multiple loads, n)	n	n (one is coupled)	n (variable inductors)	2	$n+[(2n-4)/4]$	2+2n	1+n	1+n
No. of capacitors (multiple loads, n)	$2+4n$	$2n$	$2n$	$3n-1$	1	2+2n	2n	1+2n
No. of transformers (multiple loads, n)	1 (with n sec. windings)	0	n (centre tapped)	0	0	1	0	0
Total components for each lamp	Large	Moderate	Moderate	Less	Less	Large	Moderate	Moderate
No. of LED loads tested	4	2	1	2	4	2	2	2
Power rating of all Lamps	Unequal	Unequal	–	Equal	Equal	Unequal	Unequal	Unequal
Dimming	Yes	Yes	Yes	No	Yes	Yes	Yes	Yes
Suitable for multiple loads	Yes	Yes	Yes	Yes	Yes	Yes	Yes	Yes
Independent dimming	Yes	No	–	No	No	Yes	Yes	Yes
Non-isolated	No	Yes	No	Yes	Yes	No	Yes	Yes

gain by cascading buck-boost converter with half-bridge resonant converter. But it leads to more component count and hence increased cost. Also, due to hard switching of buck-boost converter, the switching losses increase, and hence, the efficiency is less.

Table 3 describes the comparative study of the proposed configuration in contrast to existing similar LED drivers for multiple loads.[20,24-29] LED drivers in previous works[20,25,26] use transformers, suitable for isolated applications but have limitations like more number of transformers, secondary windings, inductors, and capacitors. Non-isolated LED drivers with multiple loads, reported in previous studies,[24,27-29] suffer from drawbacks like no independent dimming, less reliable, unequal output voltage gains, unable to drive loads with equal or unequal wattages/voltages. Further, LED driver in Ramakrishnareddy et al[28] requires one extra switch that increases cost and power losses as compared with the proposed configuration. Hence, when compared with conventional and existing similar topologies, the proposed configuration provides various advantages such as reduced device count, less cost, high gain for all LED loads, reduced switching loss due to soft-switching across all devices, improved efficiency, simple control technique, ability to drive multiple loads with equal or unequal voltages/wattages, and independent voltage regulation and dimming control. Thus, the proposed non-isolated half-bridge high gain configuration is well suitable for SPV/battery fed multiple load LED lighting applications.

8 | CONCLUSION

A high gain buck-boost integrated symmetrical half-bridge non-isolated LC series resonant converter is proposed for SPV/battery fed multiple load LED lighting applications. The integrated buck-boost operation provides optimum utilization of input voltage and results in twice the gain of the conventional half-bridge converter. Frequency modulation is used to regulate the output voltage against input voltage variations. The proposed converter configuration for single load and its extended version for two loads are realized and tested. Independent voltage regulation and dimming control are achieved for both loads. When compared with existing similar topologies, the proposed configuration provides various advantages such as reduced device count, less cost, high gain for all LED loads, reduced switching loss due to soft-switching across all devices, improved efficiency, simple control technique, ability to drive multiple loads with equal or unequal voltages/wattages, and independent voltage regulation and dimming control. Hence, the proposed non-isolated half-bridge high gain configuration is well suitable for SPV/battery fed multiple load LED lighting applications.

ORCID

Venkata Kondala Satyakar Veeramallu https://orcid.org/0000-0001-9016-1876
Porpandiselvi S. https://orcid.org/0000-0002-0168-2141
Narasimharaju B. L. https://orcid.org/0000-0002-3033-5712

REFERENCES

1. Castro I, Vazquez A, GLamar D, Arias M, Hernando MM, Sebastián J. An electrolytic capacitorless modular three-phase AC-DC LED driver based on summing the light output of each phase. *IEEE J Emerg Sel Top Power Electron*. 2019;7:2255-2270.
2. Hu Y, Jovanovic MM. LED driver with self-adaptive drive voltage. *IEEE Trans Power Electron*. 2008;23(6):3116-3125.
3. Chiu H-J, Lo Y-K, Cheng S-J, et al. A single-stage LED lamp driver with low DC bus voltage for general lighting applications. *Int J Circ Theory Appl*. 2011;39(11):1161-1175.
4. Kim J-W, Choe J-M, Lai J-SJ. Non-isolated single-switch two-channel LED driver with simple lossless snubber and low-voltage stress. *IEEE Trans Power Electron*. 2017;33(5):4306-4316.
5. Lee S-W, Choe H-J, Yun J-J. Performance improvement of a boost LED driver with high voltage gain for edge-lit LED backlights. *IEEE Trans Circ Syst II Express Briefs*. 2017;65(4):481-485.
6. Qu X, Wong S-C, Chi KT. An improved LCLC current-source-output multistring LED driver with capacitive current balancing. *IEEE Trans Power Electron*. 2014;30(10):5783-5791.
7. Ramakrishnareddy Ch K, Porpandiselvi S, Vishwanathan N. An efficient full-bridge resonant converter for light emitting diode (LED) application with simple current control. *Int J Circ Theory Appl*. 2019.
8. Reddy CKR, Porpandiselvi S, Satyakar VVK. Input controlled series-resonant converter for LED lighting application. In: 3rd International Conference on Communication and Electronics Systems (ICCES). IEEE; 2018; Coimbatore, India, India:608-612.
9. Arias Pérez de Azpeitia M, Castro Álvarez I, González Lamar D, Vázquez Ardura A, Sebastián Zúñiga FJ. Optimized design of a high input-voltage-ripple-rejection converter for LED lighting. *IEEE Trans Power Electron*. June 2018;6:5192-5205.
10. Borekci S, Acar NC, Kircay A. LED dimming technique without frequency and pulse width modulations. *Int J Circ Theory Appl*. 2018;46(11):2028-2037.

11. Gücin TN, Fincan B, Biberoğlu M. A series resonant converter-based multichannel LED driver with inherent current balancing and dimming capability. *IEEE Trans Power Electron*. 2018;34(3):2693-2703.
12. Mounika D, Porpandiselvi S. ADC controlled parallel loaded resonant half-bridge converter for LED lighting. In: 2017 2nd International Conference on Communication and Electronics Systems (ICCES). IEEE; 2017; Coimbatore, India:1031-1036.
13. Porpandiselvi S, Mounika D. ADC controlled half-bridge LC series resonant converter for led lighting. In: 2017 2nd International Conference on Communication and Electronics Systems (ICCES). IEEE; 2017; Coimbatore, India:1037-1042.
14. Ye C, Das P, Sahoo SK. Peak current control of multichannel LED driver with selective dimming. *IEEE Trans Indust Electron*. 2018;66(5):3446-3457.
15. Cheng C-A, Chung T-Y. A single-stage LED streetlight driver with PFC and digital PWM dimming capability. *Int J Circ Theory Appl*. 2016;44(11):1942-1958.
16. Ma H, Li Y, Chen Q, Zhang L, Xu J. A single-stage integrated boost-LLC AC–DC converter with quasi-constant bus voltage for multichannel LED street-lighting applications. *IEEE J Emerg Sel Top Power Electron*. 2018;6(3):1143-1153.
17. Malschitzky A, Albuquerque F, Agostini E, Nascimento CB. Single-stage integrated bridgeless-boost nonresonant half-bridge converter for LED driver applications. *IEEE Trans Indust Electron*. 2017;65(5):3866-3878.
18. Wang Y, Deng X, Wang Y, Xu D. Single-stage bridgeless LED driver based on a CLCL resonant converter. *IEEE Trans Indust Appl*. 2017;54(2):1832-1841.
19. Wang Y, Hu X, Guan Y, Xu D. A single-stage LED driver based on half-bridge CLCL resonant converter and buck–boost circuit. *IEEE J Emerg Sel Top Power Electron*. 2018;7(1):196-208.
20. Alonso JM, Perdigao MS, Dalla Costa MA, Martínez G., Osorio R. Analysis and experiments on a single-inductor half-bridge LED driver with magnetic control. *IEEE Trans Power Electron*. 2017;32(12):9179-9190.
21. Jeong Y, Kim J-K, Lee J-B, Moon G-W. An asymmetric half-bridge resonant converter having a reduced conduction loss for DC/DC power applications with a wide range of low input voltage. *IEEE Trans Power Electron*. 2016;32(10):7795-7804.
22. Lin L, Xu J, Chen Y, Wang X, Cao J. Asymmetrical hybrid-controlled half-bridge LCC resonant converter with low conduction loss and wide ZVS operation range. *Electron Lett*. 2017;53(21):1422-1424.
23. Satyakar VVK, Porpandiselvi S, Reddy CKR. Buck-boost based parallel resonant converter for multiple load LED lighting application. In: 2018 Third International Conference on Electrical, Electronics, Communication, Computer Technologies and Optimization Techniques (ICEECCOT). Mysuru, India: IEEE; 2018:72-77.
24. Hwu K, Jiang W. Non-isolated two-phase interleaved LED driver with capacitive current sharing. *IEEE Trans Power Electron*. 2017;33(3):2295-2306.
25. Liu J, Sun W, Zeng J. Precise current sharing control for multi-channel LED driver based on switch-controlled capacitor. *IET Power Electron*. 2017;10(3):357-367.
26. Luo Q, Zhi S, Zou C, Zhao B, Zhou L. Analysis and design of a multi-channel constant current light-emitting diode driver based on high-frequency AC bus. *IET Power Electron*. 2013;6(9):1803-1811.
27. Ramakrishnareddy CK, Shunmugam P, Vishwanathan N. Soft switched full-bridge light emitting diode driver configuration for street lighting application. *IET Power Electron*. 2017;11(1):149-159.
28. Ramakrishnareddy Ch K, Porpandiselvi S, Vishwanathan N. A three-leg resonant converter for two output LED lighting application with independent control. *Int J Circ Theory Appl*. 2019;47(7):1173-1187.
29. Reddy UR, Narasimharaju BL. A cost-effective zero-voltage switching dual-output LED driver. *IEEE Trans Power Electron*. 2016;32(10):7941-7953.
30. Steigerwald RL. A comparison of half-bridge resonant converter topologies. *IEEE Trans Power Electron*. 1988;3(2):174-182.

How to cite this article: Veeramallu VKS, S P, BL N. A buck-boost integrated high gain non-isolated half-bridge series resonant converter for solar PV/battery fed multiple load LED lighting applications. *Int J Circ Theor Appl*. 2020;48:266-285. https://doi.org/10.1002/cta.2720